ADVANCED SUSTAINABLE SYSTEMS
www.advsustainsys.com

Comparative Evaluation of Different MOF and Non-MOF Porous Materials for SO_2 Adsorption and Separation Showing the Importance of Small Pore Diameters for Low-Pressure Uptake

*Philipp Brandt, Alexander Nuhnen, Seçil Öztürk, Gülin Kurt, Jun Liang, and Christoph Janiak**

Dedicated to Prof. Wolfgang Kaim on the occasion of his 70th birthday

The search for adsorbents for flue gas desulfurization processes is a current interest. For the first time, a comparative experimental study of SO_2 adsorption by porous materials including the prototypical metal–organic frameworks NH_2-MIL-101(Cr), Basolite F300 (Fe-1,3,5-BTC), HKUST-1 (Cu-BTC), the zeolitic imidazolate frameworks (ZIF)-8, ZIF-67, the alumosilicate Zeolite Y, the silicoaluminumphosphate (SAPO)-34, Silica gel 60, the covalent triazine framework (CTF)-1, and the active carbon Ketjenblack is carried out. Microporous materials with pore sizes in the range of 4–8 Å or with nitrogen heterocycles are found to be optimal for SO_2 uptake in the low-pressure range. The SO_2 uptake capacity at 1 bar correlates with the Brunauer-Emmett-Teller-surface area and pore volume rather independently of the surface microstructure. Zeolite Y and SAPO-34 are stable toward humid SO_2. The materials Zeolite Y and CTF-1(600) show the most promising SO_2/CO_2 selectivity results with an ideal adsorbed solution theory selectivity in the range of 265–149 and 63–43 with a mole fraction of 0.01–0.5 SO_2, respectively, at 293 K and 1 bar.

1. Introduction

Over 85% of the global energy is still generated from the burning of fossil fuels leading to the emission of exhaust fumes, containing CO_2, NO_x, and SO_2.[1,2] For example, 43% of total SO_2 emissions (62.7 Mt in 2018) are related to coal combustion (27.0 Mt in 2018).[3] Emission of the toxic and acidic anhydrate gas SO_2 is harmful to the biosphere and to human health both through air pollution and the formation of acid rain.[4,5]

The classic separation of SO_2 from flue gases is done by wet limestone-scrubbing or treatment by amine-based absorbents.[6] Flue gases generated by heavy oil- or coal combustion typically contain 500–3000 ppm of SO_2, which can be reduced by up to 95% using these established methods.[7] Importantly, traces of SO_2 of <500 ppm remain in the flue gas and are emitted into the atmosphere. Also, this residual SO_2 inactivates CO_2 adsorbents or poisons selective NO_x-oxidation catalysts.[8–10] A further decrease of the SO_2 content in flue gases is therefore of high economic and environmental importance. Reversible SO_2 physisorption by porous materials is seen as a means to achieve a further SO_2 reduction in flue gases.

Currently, the SO_2 adsorption with metal–organic frameworks (MOFs) experiences high interest.[11–27] Metal–organic frameworks are typically microporous metal-ligand coordination networks with uniform porosity, low density, and high tunability through the organic linker, that is, the metal-bridging ligand.[28] MOFs are actively studied in the role of adsorbents (particularly N_2, H_2, CO_2, CH_4, etc.) for prospective gas storage and gas separation[29–31] or the capture of toxic and polluting gases.[32–38] Yet, MOFs are often not of high chemical and hydrothermal stability.[39] An advantage of MOFs is clearly their designability, in particular their controllable pore size and modifiable pore surface is unmatched, yet, other porous materials may also feature good SO_2 uptake characteristics.

The main components of a typical flue gas mixture are N_2 or CO_2 with a minor part of SO_2 (500–3000 ppm).[7] Superior affinity to SO_2 over CO_2 and N_2, which conditions high selectivity, is essential for reaching high efficiency of separation. A promising material should also possess a high SO_2 single-gas

P. Brandt, Dr. A. Nuhnen, S. Öztürk, G. Kurt, Dr. J. Liang, Prof. C. Janiak
Institut für Anorganische und Analytische Chemie
Heinrich-Heine-Universität Düsseldorf
Düsseldorf 40204, Germany
E-mail: janiak@uni-duesseldorf.de
Dr. J. Liang, Prof. C. Janiak
Hoffmann Institute of Advanced Materials
Shenzhen Polytechnic
7098 Liuxian Blvd, Nanshan District, Shenzhen 518055, China
The ORCID identification number(s) for the author(s) of this article can be found under https://doi.org/10.1002/adsu.202000285.

DOI: 10.1002/adsu.202000285

adsorption capacity in the low-pressure range without appreciable hysteresis. The overall potential of an SO_2 adsorbent depends also on stability and recyclability. SO_2 sorption materials should withstand corrosive conditions under dry and humid SO_2 exposure without a decrease in adsorption capability.[40] Further, the reversibility of the SO_2 adsorption at near room temperatures and energy-efficient recovery is crucial.[41] The prospective porous materials for reversible physisorption should be microporous (d_{pore} < 2 nm), as adsorption should occur at low pressures to secure the removal of the relevant trace amounts of SO_2 from flue gases.[41]

In view of the current high interest on the physisorption of SO_2 with MOFs we are critically comparing here selected MOFs with other selected porous materials, namely the alumosilicate Zeolite Y, the silicoaluminumphosphate (SAPO)-34, Silica gel 60, the covalent triazine framework (CTF)-1, and the active carbon Ketjenblack. The collected SO_2 adsorption data were used to verify existing simulation calculations[42–44] and assess the materials for their capabilities to remove low SO_2 concentrations from $N_2/CO_2/SO_2$ gas mixtures, with quantitative assessment of SO_2/CO_2 selectivities using the ideal adsorbed solution theory (IAST) model. Furthermore, the relative stabilities toward dry and humid SO_2 gas were determined via a follow-up porosity and powder X-ray diffraction pattern analysis.

2. Results and Discussion

We selected the MOFs NH_2-Matériaux de l'Institut Lavoisier (MIL)-101(Cr)[45,46], Basolite F300[47,48] (also named Fe-1,3,5-benzenetricarboxylate (BTC)), Hong Kong University of Science and Technology (HKUST)-1[49,50] (also named Cu-BTC), the zeolitic imidazolate frameworks (ZIF)-8,[51,52] and ZIF-67[53,54] which can all be considered highly prototypical and which are intensely investigated toward application-oriented properties (see the Supporting Information for information on their structure). From the other porous material classes Zeolite Y,[55] the silicoaluminum phosphate SAPO-34,[56] Silica gel 60, the carbon–nitrogen framework CTF-1[57] (covalent triazine framework), and the active carbon Ketjenblack were investigated for SO_2 physisorption. Ketjenblack is a form of active carbon with high electroconductivity and a broad pore size distribution with a somewhat more ordered structure compared to other active carbons.[58,59] With this selection of materials we aim to cover a broad range of properties, e.g., pore size, functionality, open metal sites, etc. for comparative purposes (see Section S1, Supporting Information, for details). The MOFs NH_2-MIL-101(Cr), HKUST-1, ZIF-8, and ZIF-67 were synthesized according to literature procedures and their identity was established by powder X-ray diffractometry (PXRD) and porosity analysis from nitrogen sorption isotherms (see the Supporting Information for details). The materials Basolite F300, Zeolite Y, SAPO-34, Silica gel 60, and Ketjenblack were purchased from commercial sources (see the Supporting Information for further information).

The individual SO_2 adsorption isotherms were measured at 293 K (**Figures 1** and **2**, for a combination, see Figure S22, Supporting Information) and the corresponding data together with the porosity characteristics from nitrogen sorption isotherms is given in **Table 1**. For clarity in the SO_2 sorption isotherm diagrams we will present and discuss the MOF and the non-MOF materials separately.

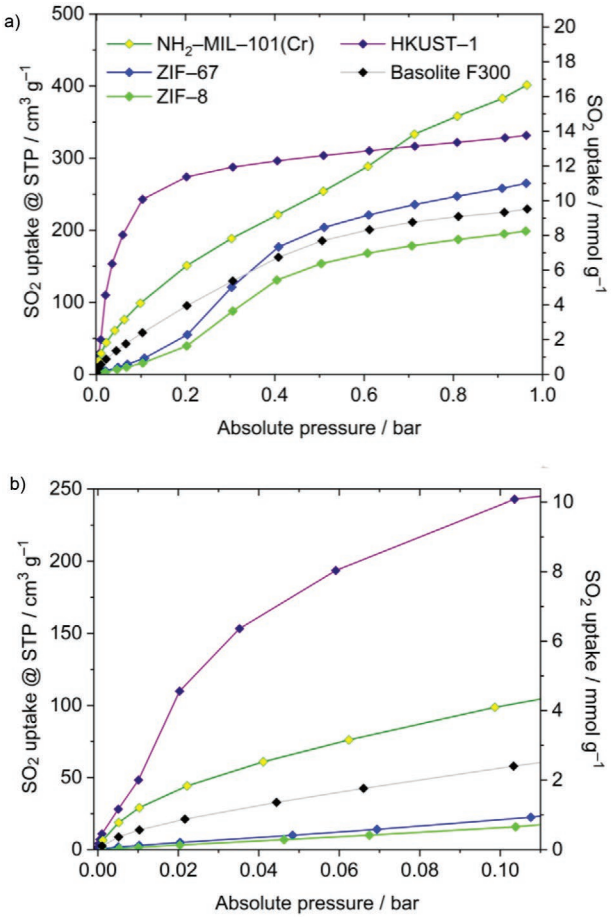

Figure 1. SO_2 adsorption isotherms (293 K) of the examined MOF materials: a) 0.001–1 bar and b) 0.001–0.11 bar. SO_2 desorption isotherms are omitted for clarity and are displayed in Figures S23–S29 in the Supporting Information.

2.1. SO_2 Adsorption by MOF Materials

The amino-functionalized MOF NH_2-MIL-101(Cr) shows a moderate rise in SO_2 uptake in the pressure range from 0.001 to 0.1 bar with an SO_2 uptake of 4.1 mmol g^{-1} at 0.1 bar. The SO_2 isotherm reflects a steady increase up to ambient pressures with a maximum SO_2 uptake of 16.7 mmol g^{-1} at 1 bar without reaching a saturation stage. The adsorption isotherm is far from leveling off at 1 bar. This can be explained by relatively large micropores with a diameter of 15.4 and 19.9 Å for NH_2-MIL-101(Cr) (vide infra).[70]

The amino functionalization of the MOFs was chosen as a possible factor, favoring adsorption of SO_2, interpretable both as an interaction between basic and acidic species or as an interaction between polar species with enhanced dipole–dipole interactions.[19] Interestingly, however, NH_2-MIL-101(Cr) shows no surface-specific enhancement of SO_2 uptake, i.e., the uptake per unit of the Brunauer-Emmett-Teller (BET) surface (see below),

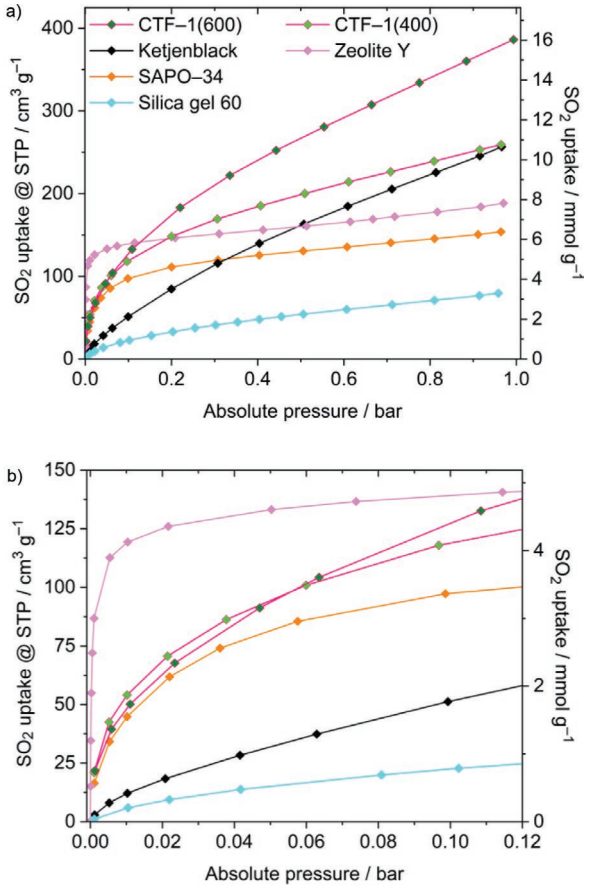

Figure 2. SO_2 adsorption isotherms (293 K) of the examined non-MOF materials: a) 0.001–1 bar and b) 0.001–0.12 bar. SO_2 desorption isotherms are omitted for clarity and are displayed in Figures S23–S29 in the Supporting Information.

compared to other materials in this study. Ibarra et al. recently investigated SO_2 adsorption in the fluorinated MIL-101(Cr)4-F which shows a roughly similar isotherm shape to the isoreticular amino-functionalized frameworks but with slightly higher SO_2 adsorption capacity with uptakes of 4.6 and 18.4 mmol g^{-1} at 0.1 and 1 bar, respectively, at 298 K and features exceptional stability against SO_2.[71] This is in agreement with a smaller enthalpy of adsorption near zero coverage, $\Delta H^0_{ads} = -36$ kJ mol^{-1} for NH_2-MIL-101(Cr) (Figure S35, Supporting Information) than $\Delta H^0_{ads} = -54$ kJ mol^{-1} for MIL-101(Cr)4-F.[71]

Basolite F300 shows somewhat lower SO_2 adsorption over the whole pressure range than NH_2-MIL-101(Cr), reaching 9.5 mmol g^{-1} at 1 bar.

The SO_2 isotherm of HKUST-1 features a single sharp increase in uptake to 10.1 mmol g^{-1} at 0.1 bar, followed by a fast transition to near saturation with a maximum SO_2 uptake of 13.8 mmol g^{-1} at 1 bar (a type-Ib isotherm by the International Union of Pure and Applied Chemistry (IUPAC) classification).[72] To the best of our knowledge HKUST-1 shows one of the highest SO_2 capacities with a type-I isotherm under ambient temperature and pressure ever reported. The remarkable uptake of HKUST-1 can be explained by the abundance of open metal sites (coordinatively unsaturated copper sites).[73] Our experimental results are in good agreement with simulation calculations for SO_2 in HKUST-1 carried out by Song et al. (sim./exp. at 298/293 K at 0.05 bar = ≈0.9/0.8 mmol g^{-1} or 1 bar = ≈15/13.8 mmol g^{-1})[44] where absolute values deviate only slightly due to differences in accessible surface area. However, in subsequent stability tests, HKUST-1 showed no sustained stability (see below).

ZIF-8 and ZIF-67 both feature an unusual "S"-shaped (IUPAC type-V isotherm)[72] adsorption isotherm, with an initial stage at ≤ ≈0.1 bar where the adsorption is very low. The delayed SO_2 uptake for ZIF-8 was previously predicted by Sun et al. and Song et al. by simulation calculations and is in good agreement

Table 1. SO_2 adsorption data and porosity characteristics at 293 K.

Material	Formula	SO_2 uptake [mmol g^{-1}] at			BET[a)] [m^2 g^{-1}]	Total pore vol.[b)] [cm^3 g^{-1}]	Pore width[c)] [Å]	SO_2/CO_2 selectivity[d)] at SO_2/CO_2 molar ratio		
		0.01 bar	0.1 bar	1 bar				0.01	0.1	0.5
NH_2-MIL-101(Cr)	$[Cr_3(O)(OH)(NH_2\text{-bdc})_3(H_2O)_2]$	1.2	4.1	16.7	2290	1.16	15.4, 19.9[70]	34	30	30
Basolite F300; Fe(BTC)	n.a.	0.6	2.4	9.5	1070	0.49	18–22[60]	n.d.	n.d.	n.d.
HKUST-1	$[Cu_3(1,3,5\text{-btc})_2(H_2O)_3]$	2.0	10.1	13.8	1490	0.61	5, 11, 14[61]	41	36	28
ZIF-8	$Zn(2\text{-MeIm})_2$	0.1	0.7	8.2	1820	0.80	3.4, 11.4[75]	n.d.	n.d.	n.d.
ZIF-67	$Co(2\text{-MeIm})_2$	0.1	0.9	11.0	1980	0.69	3.4, 11.4[75]	n.d.	n.d.	n.d.
Zeolite Y (NaY)	n.a.	5.0	5.8	7.7	930	0.33	7.4, 13.7[62]	265	180	149
SAPO-34	n.a.	1.9	4.0	6.4	720	0.28	≈5[63]	42	36	33
Silica gel 60	n.a.	0.2	0.9	3.3	540	0.75	≈10–100, av. 60[64]	n.d.	n.d.	n.d.
CTF-1(400)	Ideally $(C_8H_4N_2)_x$	2.2	4.9	10.8	980	0.46	≈6–25[65,66]	62	40	27
CTF-1(600)	Ideally $(C_8H_4N_2)_x$	2.1	5.5	16.0	2060	1.20	≈8–35[66,67]	63	46	43
Ketjenblack	Ideally C	0.5	2.1	10.7	1410	1.24	≈20–80, av. 40[68,69]	9	10	14

[a)]BET areas were calculated from five adsorption points of the N_2 isotherms within $0.05 < p\ p_0^{-1} < 0.2$. Values were rounded according to the estimated standard deviation of ±20 m^2 g^{-1}; [b)]Total pore volumes were calculated from experimental N_2 sorption data at $p\ p_0^{-1} = 0.85$–0.95, depending on the isotherm shape. For details see Section S2.3 in the Supporting Information; [c)]Pore widths as given in the literature; [d)]See Section S2.5 in the Supporting Information for the CO_2 sorption data. The MOFs Basolite F300, ZIF-8, ZIF-67, and Silica gel 60 did not show an appreciable SO_2 uptake at low pressure, hence the SO_2/CO_2 selectivities were not determined (n.d.).

with our experimental results.[43,44] The observation of "S"-isotherm shapes can be explained by the small pore entrance diameter of 3.4 Å[74,75] for both ZIF-8 and ZIF-67 and hence steric hindrance for the passage of SO_2 (kinetic diameter of 4.1 Å).[76]

The gate-opening effect occurring in both ZIFs, where the methyl groups of the ligand rotate due to the swinging of the imidazolate rings,[77] is the reason for the delayed rise in SO_2 adsorption occurs at ≈0.3 bar for both ZIF-8 and ZIF-67. The maximum SO_2 uptake reaches 8.2 and 11.0 mmol g^{-1} at 1 bar, respectively.

2.2. SO_2 Adsorption by Non-MOF Zeolite Y, SAPO-34, Silica Gel 60, CTF-1, and Ketjenblack

From all examined materials the previously investigated Zeolite Y[78–80] shows the highest affinity toward SO_2 with exceptional uptake of 5.0 mmol g^{-1} even at 0.01 bar (65% of the 1 bar capacity) with a fast transition into near saturation and maximum SO_2 uptake of 7.7 mmol g^{-1} at 1 bar.

SAPO-34 shows a type-Ib SO_2 adsorption isotherm with an uptake of 4.0 mmol g^{-1} at 0.1 bar, followed by a saturation stage with a maximum SO_2 uptake of 6.4 mmol g^{-1} at 1 bar. The adsorption differences in Zeolite Y and SAPO-34 which have a broadly similar structure correlate rather well with the difference in surface area and pore volume. The high early uptake of both materials can be traced to their small pore sizes which favor multiple SO_2-pore wall interactions (see below).

Silica gel 60 demonstrated a steady linear rise of SO_2 adsorption reaching an uptake of 3.3 mmol g^{-1} at 1 bar, which is the lowest value in this comparative study. The effect could be explained by the combination of relatively low surface area and large pore sizes of the chiefly mesoporous Silica gel, which worsens the efficiency of the host–guest interactions. The saturation stage should be reached at pressures exceeding 1 bar.

The two covalent triazine frameworks (CTFs) CTF-1(400) and CTF-1(600) are synthesized at 400 and 600 °C, respectively. CTF-1(400) and CTF-1(600) show steep uptake steps with 4.9 and 5.5 mmol g^{-1} adsorbed at 0.1 bar, followed by a nearly linear uptake reaching the values of 10.8 and 16.0 mmol g^{-1} at 1 bar, respectively. Ketjenblack has a nearly linear uptake over the whole pressure range and arrives at an uptake of 10.7 mmol g^{-1} at 1 bar. Neither of the three carbon materials reaches the saturation at 1 bar. Especially, the isotherms for CTF-1(600) and Ketjenblack still have a high positive slope and are far from leveling off at 1 bar. The superior affinity of the CTFs to SO_2 compared to Ketjenblack is likely due to the presence of smaller pore sizes in the former and more importantly due to stronger dipole–dipole interaction between the triazine and nitrile nitrogen atoms and SO_2. The nitrogen atoms are primarily heteroarylic, but residual, unreacted terminal nitrile groups are also present.[81]

2.3. Structure–Adsorption Relationships

The surface area and the total accessible pore volume could be taken as the two primary factors governing the total SO_2 adsorption at 1 bar. The SO_2 uptake of all examined materials at 293 K and 1 bar is plotted against the BET-surface area and the pore volume in **Figure 3**. The examined materials differ significantly in terms of chemical composition and surface microstructure, nevertheless, the microporous materials without diffusion restriction show a reasonable correlation between SO_2 uptake and BET-surface area and total pore volume (Figure 3).

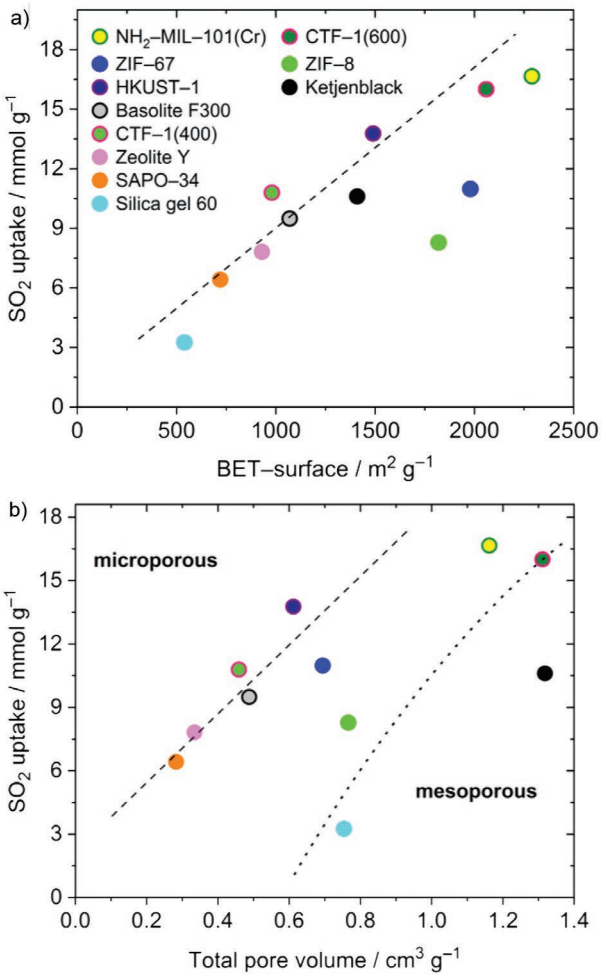

Figure 3. SO_2 uptake (1 bar, 293 K) versus a) BET-surface area and b) total accessible pore volume (both determined by N_2 adsorption at 77 K). The dashed trend lines are a guide to the eye. The dotted line in (b) separates the micro- and mesoporous materials.

The two microporous ZIFs are noteworthy outliers in the uptake-surface area and pore volume correlation. This can be explained with the noted small pore window diameter of 3.4 Å[74,75] and steric hindrance for the passage of SO_2. Above the threshold or gate-opening pressure of ≈0.3 bar, the SO_2 molecules could enter the pores. The two ZIFs are microporous materials with no mesopores. However, when probing the BET surface area, the smaller N_2 molecule with its kinetic diameter of 3.64 Å can more effectively cover the surface and fill the 11.4 Å diameter pore, than the larger SO_2 molecule with its kinetic diameter of 4.1 Å. Part of the pore surface and volume will remain inaccessible or empty with SO_2 due to steric hindrance from nearby adsorbates. A geometric estimate suggests that about 6 SO_2 molecules may fit into the 11.4 pore, while about 15 N_2 molecules can fill the same space. This effect of inaccessible surface is

especially pronounced in pores wider than the molecule length, but not wide enough for unrestrained surface coverage.

Also, the uptake of NH_2-MIL-101(Cr), CTF-1(600), Ketjenblack, and Silica gel 60 is lower than expected from their surface area or pore volume which corresponds to the not reached saturation stage at 1 bar (see their above sorption isotherms). The total pore volume represents the limit for the maximum capacity. This is why the (partially) mesoporous materials are positioned below the linear trend line of the uptake versus surface area and pore volume dependence. The larger pores are not completely filled as the adsorption curve is far from saturation (in terms of an idealized Langmuir curve). The saturation uptake is only reached at pressures higher than 1 bar. The pore filling of such larger mesopores would have to occur by (framework-)O=S···O=S=O and (framework-)O=S=O···S=O dipole–dipole interactions, forming SO_2 chains or clusters. The dipole moment of SO_2 plays an important role in the adsorption process. In mesopores only part of the adsorbed SO_2 can interact with the surface. If in addition the surface of the mesoporous materials has only low affinity sites (e.g., Ketjenblack, Silica gel 60) then this contributes to the not reached saturation.

Most applications, including flue gas desulfurization or gas sensors, are restricted to gas mixtures with low partial pressures of SO_2. The optimization of the material performance at low pressures (≤ 0.1 bar) is therefore essential, whereas the total accessible pore volume should only be nonlimiting, i.e., only a certain threshold for the minimal uptake should be guaranteed. For the targeted low-pressure region, it is evident that there is no correlation between low-pressure SO_2 uptake and BET surface area (Figure S30, Supporting Information) and there is also no correlation of the SO_2 uptake to the micropore volume (Figure S31, Supporting Information).

For a high gas uptake at low pressure, that is a type-I isotherm, there must be a high affinity between the adsorbent and the adsorbate. At low pressure, the adsorption affinity is synonymous with the uptake as long as the latter is not limited by surface area or accessible volume. The SO_2 adsorption isotherms of the materials were fitted with a Langmuir (LAI) or dual-site Langmuir (DSL) model yielding the affinity constants given in **Table 2**. The remarkably high initial SO_2 affinity constant of Zeolite Y (2739 bar^{-1}) correlates with the higher initial uptake compared to SAPO-34 or CTF-1(400/600) with less steep uptake und thus yielding lower SO_2 affinity constants (95, 143, and 115 bar^{-1}, respectively).

Table 2. Fitting parameters for SO_2/CO_2 IAST-selectivities at 293 K.

Material[a)]	Gas	Model[b)]	Affinity const. [bar^{-1}]
NH_2-MIL-101(Cr)	SO_2	DSL	46.0
	CO_2	DSL	9.6
HKUST-1	SO_2	LAI	22.0
	CO_2	LAI	0.4
SAPO-34	SO_2	DSL	95.1
	CO_2	DSL	5.5
Zeolite Y	SO_2	DSL	2739
	CO_2	DSL	9.3
CTF-1(400)	SO_2	DSL	143.3
	CO_2	DSL	6.1
CTF-1(600)	SO_2	DSL	115.3
	CO_2	DSL	10.5
Ketjenblack	SO_2	LAI	0.9
	CO_2	LAI	0.4

[a)]Basolite F300, ZIF-8, ZIF-67, and Silica gel 60 were not included in the IAST calculations for their low SO_2 uptakes at low pressures. The correlation coefficients for the isotherm fits were >0.996; [b)]DSL = Dual-site Langmuir; LAI = Langmuir.

There is an optimum (or local optima) of pore size and pore shape for a given molecule. For example, one local optimum for a linear gas molecule with a length of L_{ads} is an adsorbent structure with opposite surfaces at a distance of L_{ads} between the Connolly surface, i.e., probe the accessible surface of the opposite sides.[72] This ensures optimal dispersive interactions with both ends of the molecule to the surface and this model is often used for computations.

The results of this study support the existence of an optimal pore size[18,26] for a high adsorption affinity of SO_2 at low pressures. The existence of such optimum is clearly visible by the maximum in the distribution of the surface-specific SO_2 uptake at 0.01 bar and 0.1 bar (293 K) against the pore limiting diameter (PLD), shown in **Figure 4**. As the absolute value of the uptake at low pressure depends on the surface area, it was normalized by division through the surface area, giving the surface-specific SO_2 uptake.

The PLD is the smallest diameter of a pore or window, present in a framework. The optimum pore width would be ≈4–8 Å, as found in HKUST-1, Zeolite Y, SAPO-34, and CTF-1(400). Porous materials with such pore widths exhibit a surface-specific SO_2 uptake larger than 1×10^{-3} or 5×10^{-3} mmol m^{-2} at 0.01 or 0.1 bar, respectively. In contrast, materials with pores outside the above pore criteria exhibit a surface-specific SO_2 uptake smaller than 0.5×10^{-3} or 2×10^{-3} mmol m^{-2} at 0.01 or 0.1 bar, respectively.

Grand-canonical Monte Carlo (GCMC) simulations for SO_2 sorption in MOFs, among them HKUST-1 and ZIF-8, also indicated that the amount of SO_2 adsorbed at 1 bar correlated neither well with the surface area nor with the total accessible pore volume. Instead, a good correlation of SO_2 uptake was found with the heat of adsorption in small pore ($d_{pore} \geq 4$ Å) materials at 0.05 bar pressure.[44]

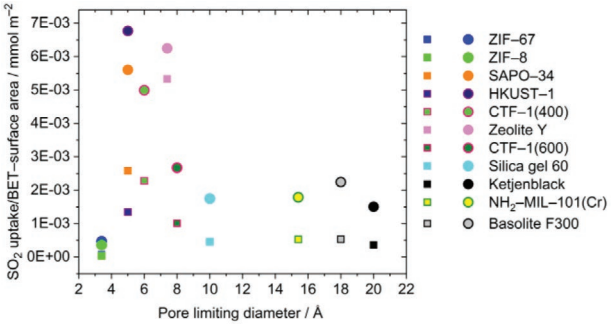

Figure 4. Surface specific SO_2 uptake (i.e., the total uptake divided/normalized by the BET-surface area) at 0.01 bar (squares) and 0.1 bar (circles) versus the pore limiting diameter. Note that for Silica Gel 60, CTF-1, and Ketjenblack only the smallest pore diameter is indicated and these materials have a broad pore size distribution (Table 1).

Furthermore, studies on NH_2-MIL-125(Ti) and $[Zn_2(L1)_2(bpe)]$ indicate a positive effect of nitrogen functionalization to enhance the SO_2 affinity at low pressures.[26,82] The effect could be operating here for CTF-1(400), CTF-1(600), and NH_2-MIL-101(Cr) and partially offset the (expected) lower uptake from the larger pore diameters.

In situ inelastic neutron scattering and density functional theory (DFT) calculations of SO_2 at manchester framework material (MFM)-300(Al)[19] and in situ synchrotron PXRD studies on MFM-601(Zr)[83] had shown that stronger SO_2 anchor points are also metal-OH groups as the hydrogen-bonding sites (metal-OH···O=S=O) for the first SO_2 molecules. Here NH_2-MIL-101(Cr) and most likely Basolite F300 feature metal-OH anchor points. Also, the open metal sites in HKUST-1 are strong binding sites. However, in situ SO_2 sorption synchrotron single-crystal X-ray diffraction experiments on the Cu(II) paddle-wheel MOF MFM-170 gave the open Cu^{2+} sites only as the secondary adsorption sites, where the SO_2 molecule binds to in an end-on mode Cu···O=S=O with 2.3(1) Å and an occupancy of only 0.67. Upon desorption the diffraction data under a dynamic vacuum at 298 K left the Cu^{2+}-bound SO_2 with an occupancy of 0.09 which suggests that due to the Jahn–Teller effect the Cu-O=S=O bonding is weak so that it is almost entirely desorbed on the reduction of pressure.[21] On the other hand, ZIF-8 and ZIF-67 neither have metal-OH nor open metal sites, contributing to a low affinity, besides the low uptake due to the gate-opening effect (vide supra).

2.4. IAST Selectivity

CO_2 is the main competitor of SO_2 regarding the binding to the adsorbent during the flue gas desulfurization. The SO_2/CO_2 selectivity, which is crucial for the separation of gas mixtures, was assessed with the IAST model for some of the most promising materials using binary SO_2/CO_2 mixtures. IAST-based estimations are adequate when the conditions of low relative pressures, similar polarity, as well as close molecular volumes of the components of the gas mixture, are fulfilled.[84]

The calculation of IAST-selectivities was performed by fitting the adsorption isotherm data points (Figures S23–S29 and Table S2, Supporting Information) using the "3P sim" software (parameters in Table S3, Supporting Information).[85]

The dependence of the calculated SO_2/CO_2 IAST-selectivities on the mole fraction of SO_2 (1 bar, 293 K) for all the examined materials are shown in **Figure 5**. Along with the order of Zeolite Y, CTF-1(600), CTF-1(400), SAPO-34, and HKUST-1 with SO_2/CO_2 IAST-selectivities from 265, 63, 62, 42, and 41 these materials demonstrated the highest selectivities at 0.01 (10.000 ppm) molar fraction of SO_2 (293 K and 1 bar). It is interesting that at a higher SO_2 molar fraction of 0.5, the respective values become 149, 43, 27, 33, and 28 (293 K and 1 bar), i.e., the order changes somewhat. Overall, Zeolite Y shows the most promising result regarding the capture of SO_2 from flue gas mixtures since it provides a high SO_2/CO_2 selectivity and its type-I isotherm should allow a relatively small pressure interval for pressure swing adsorption processes.

Although, HKUST-1 shows decent SO_2/CO_2 selectivity of 41 at a 0.01 molar fraction of SO_2, previously, Yaghi et al. and

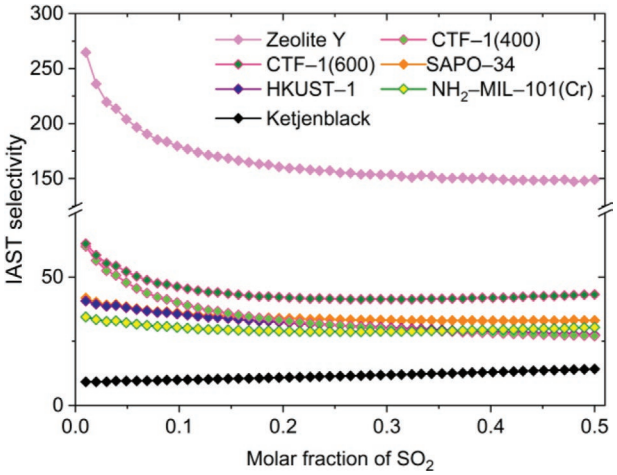

Figure 5. SO_2/CO_2 IAST selectivity dependence on the molar fraction of SO_2 in the range of 0.01–0.5 (293 K, 1 bar).

Jones et al. used HKUST-1 in breakthrough experiments in which the material showed no significant retention of SO_2.[32,86] Furthermore, a decreasing IAST-selectivity of HKUST-1 toward even lower SO_2 partial pressures than 0.01 indicates that the material might not be able to separate trace amounts of SO_2. Noteworthy, HKUST-1 had the highest calculated selectivity for NO_x from GCMC simulations on a broad range of porous materials, including MOFs, ZIFs and zeolites with respect to a gas mixture of CO_2, N_2, O_2, SO_2, and NO_x.[43]

Despite the high surface area of Ketjenblack the low affinity to SO_2 results in its unremarkable SO_2/CO_2 IAST-selectivity of 9 at a 0.01 molar fraction of SO_2 (293 K and 1 bar).

2.5. Stability Test toward Dry and Moist SO_2

Stability tests of investigated materials were carried out with both dry and humid SO_2 (the experimental methodology is given in the Supporting Information). From thermogravimetric analysis the porous materials show an initial water loss from their pores, but the frameworks are stable to 300 °C (Figures S32 and S33, Supporting Information). Humid SO_2, containing the moderately strong and quite corrosive sulfurous acid in equilibrium, reflects much better the real-world conditions in a potential sequestration application. The change of the BET-surface area and the total pore volume after SO_2 exposure during the specified time was used as the primary stability indicator parameters (**Figure 6** and Figures S11–S21, Supporting Information), while changes of the PXRD patterns were examined qualitatively (Figures S4–S10, Supporting Information). Note that the influence of humid SO_2 exposure was mainly examined for materials that demonstrated both notable stability under dry SO_2 exposure and remarkable SO_2 affinity. While ZIF-8, ZIF-67, and Silica gel 60 were very stable toward dry SO_2 (Figure 6), their affinity was low, hence neither of the three was subjected to humid SO_2 anymore. It is worth mentioning that changes in the PXRD pattern were less prominent upon decomposition which is why a combination of diffraction and adsorption experiments is always recommended.

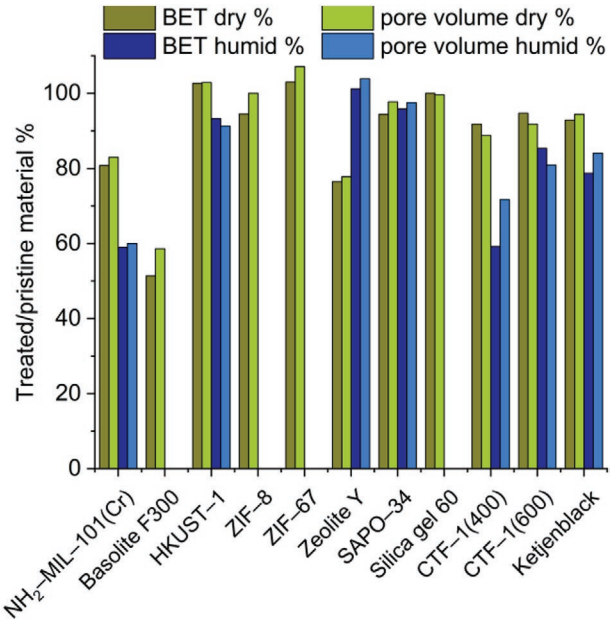

Figure 6. The relative (treated/pristine) BET surface area and total pore volume of investigated porous materials after dry and humid SO_2 exposure.

The dry SO_2 exposure during ≤10 h did not affect the majority of examined materials strongly (Figure 6). Most materials retained more than 90% of the BET-surface area and pore volume, in comparison to the untreated material. However, the amino-functionalized MOF NH_2-MIL-101(Cr) as well as Basolite F300 demonstrated a major loss of porosity and were deemed SO_2-unstable. We note that the parent MOF to NH_2-MIL-101(Cr), namely MIL-101(Cr) is also not stable toward SO_2 which was explained by its comparatively hydrophilic nature.[71] We suggest that both NH_2-MIL-101(Cr) and Basolite F300 are unstable because the SO_2 can interact with the metal-aqua and hydroxido ligand M-OH_2 and M-OH (Figure S1, Supporting Information), which are still present in both metal-cluster secondary building units (SBUs) after activation at 120 °C. Such an interaction can form sulfurous acid or hydrogen sulfite which may break the metal-carboxylate bonds with formation of metal-sulfite and the conjugated acid of the ligand. Mounfield et al. have performed in situ IR experiments on MIL-125 which confirmed the presence of bisulfite species and, in combination with computational simulations of formation energies of these adsorbed species, indicated that the degradation of the framework. The degradation likely proceeds through a reaction involving water, the dissociation of water or sulfurous or the combined reaction of sulfurous acid and water. Sulfurous acid, H_2SO_3 can be formed from SO_2 with humidity inside the MOF.[87]

Under humid SO_2 exposure (35 ± 5 ppm) during 5 h SAPO-34 showed nearly no change in porosity and could be considered stable under both dry and humid conditions (Figure 6). CTF-1(600), Ketjenblack and surprisingly, HKUST-1 demonstrated moderate surface area loss under the humid-SO_2 exposure conditions. CTF-1(400) showed a more severe loss in surface area and pore volume toward humid SO_2. When HKUST-1 was subjected to a humid SO_2 exposure time of 8 and 24 h a drastic degradation of the framework structure became visible in subsequent PXRD and N_2 adsorption analysis (Figures S6 and S13, Supporting Information). Concerning, the initial higher stability of HKUST-1 in comparison to usually regarded more stable NH_2-MIL-101(Cr) and Basolite F300 we refer again to the SBUs with their reactive metal-carboxylate bonds. The principle difference in the three SBUs is that the metal-aqua and -hydroxido ligands M-OH_2 and M-OH in NH_2-MIL-101(Cr) and Basolite F300 are normally bound ligands where reaction with the SO_2 under formation of reactive sulfurous acid or hydrogen sulfite can occur (Figure S1, Supporting Information). Whereas in HKUST-1, the aqua ligand on d^9-Cu(II) is subject to the Jahn–Teller distortion with an elongated Cu–O distance and weaker interaction (Figure S2, Supporting Information). This Cu-aqua ligand is easily removed upon activation. Further, sulfurous acid, which may still form, will also bind much weaker to Cu and thereby interact much slower with the Cu-carboxylate bonds.

Furthermore, SO_2 is also a strong reducing agent and may reduce the metal atoms in the MOFs to a lower valent state, such as Cr(II), Fe(II), and Cu(I). Upon reduction, the metal-carboxylate bonding can change more drastically, for example, high-spin d^4-Cr(II) is also subject to Jahn–Teller distortion. In this regard, it is interesting to note that in activated HKUST-1 it was observed through the spectroscopic investigation of adsorbed CO_2, CO, or NO that Cu(I) is present and coexists with Cu(II). Obviously, in HKUST the oxidation state of copper can be reduced to Cu(I) by redox treatments, using vacuum and/or reducing gases at different temperatures, albeit without noticeable framework degradation.[88–91] Hence, a higher "redox stability" could also be an explanation for the higher kinetic stability of HKUST-1 compared to the MIL frameworks.

A special case is Zeolite Y which exhibited better stability performance under humid exposure conditions than toward dry SO_2 (Figure 6). In the case of Zeolite Y, the accessibility and the location of the Na^+ counter cations to the anionic alumosilicate framework contribute largely to the adsorption properties of this material.[92] Polar molecules, like water, can induce cation redistribution and thus change adsorption properties, e.g., selectivity and capacity, significantly.[93,94] So, it might be the case that preadsorbed water blocks or rather changes the accessibility for SO_2 in our experiment.

3. Conclusions

Five prototypical MOF materials were compared with six representatives of other classes of porous materials regarding their SO_2 adsorption capabilities. A strong correlation between the SO_2 uptake at 1 bar and 293 K and BET-surface area and pore volume was observed for all microporous materials, independently of their surface microstructure. The highest affinity constants toward SO_2 at low partial pressures (0.01–0.1 bar) were registered for materials featuring pores with diameters of ≈4–8 Å, and aromatic nitrogen atoms (e.g. CTFs).

The calculated IAST-selectivities for SO_2 over CO_2 were in the range of 9–265 (at 0.01–0.5 molar fraction of SO_2), with the highest selectivity over the whole range given by Zeolite Y. Also, remarkable selectivities at low pressure were demonstrated by

CTF-1(400/600), which reflect the benefit of weakly basic acrylic nitrogens as more affine adsorption sites. When the stability toward humid SO_2 is further taken into consideration, this then leaves CTF-1(600), and SAPO-34 as the most promising materials for realistic use (i.e., humid conditions). The results of this work should raise the awareness for well-known porous material classes in the competition with currently advocated MOFs for SO_2 adsorption.

4. Experimental Section

Materials: The examined materials were synthesized according to published methods or obtained commercially (see Table S1, Supporting Information).

Gas Adsorption: BET characterization was performed on a Quantachrome *Autosorb 6* automatic gas adsorption analyzer (further instrument). SO_2 and CO_2 isotherms were measured on a Quantachrome *Autosorb iQ MP* instrument. Before each experiment, the samples were activated according to the literature (but at least 3 h of degassing and a temperature of not less than 393 K) and a $\approx 5 \times 10^{-3}$ mbar vacuum. All gases (He, N_2, SO_2, CO_2) were of ultrahigh purity (99.999%). The standard temperature and pressure volumes at 293.15 K and 101.325 kPa are reported according to the recommendation of the National Institute of Standards and Technology. The N_2 adsorption experiments for the BET surface area and pore volume determination were performed within a pressure range of 0.005–1 bar at 77 K. The SO_2 sorption experiments were performed within a pressure range of 0.001–1 bar (0.96 ± 0.007 bar) and 293 K. A Dräger *Pac 6000* electrochemical SO_2 sensor with a measuring range of 0.1–100 ppm was used for leakage testing and maintaining safe work conditions.

Powder X-Ray Diffraction: The PXRD measurements were performed on a Bruker *D2 Phaser* with a Cu-K_α-cathode source ($\lambda = 1.54182$; 30 kV, 10 mA) at room temperature. The finely ground samples were measured in the range of $5° < 2\theta < 50°$ using a low background silicon sample holder.

Thermogravimetric Analysis (TGA): TGA was performed on a Netzsch Thermo-Microbalance Apparatus TG 209 F3 Tarsus, at a heating rate of 10 K min^{-1} under a nitrogen flow. Samples were not activated before the measurement.

Stability Tests toward Dry and Moist SO_2: For the determination of the material stability under SO_2 exposure the change in BET surface area (N_2 sorption) and crystallinity (PXRD) were examined. Samples were activated as described above.

Stability tests toward dry SO_2 were carried out as the above SO_2 ad- and desorption isotherm measurement by exposing the sample between 8 h to less than 10 h under a variable pressure of 0.001–1 bar. Afterward the stability was assessed by the identity or changes in the PXRD and BET surface area and porosity.

Stability tests toward humid SO_2 were done in a self-constructed exposure chamber (Figure S2, Supporting Information), which contained a vessel of saturated sodium chloride solution (80 mL) to set a relative humidity (RH) of 75%. The chamber was filled with humid SO_2 by bubbling air through a solution of sodium hydrogen sulfite ($Na_2S_2O_5$ dissolved in water). The generated SO_2 concentration and the RH-value in the chamber were monitored by a Dräger *Pac 6000* SO_2 sensor and a *VWR TH300* hygrometer, respectively. The exposure was done at room temperature under an atmosphere containing 35 ± 5 ppm SO_2 and of 75 ± 6% RH humidity for 5 h. Experimental details and setup can be found in Section S2.1 in the Supporting Information.

Supporting Information

Supporting Information is available from the Wiley Online Library or from the author.

Acknowledgements

Open access funding enabled and organized by Projekt DEAL.

Conflict of Interest

The authors declare no conflict of interest.

Data Availability Statement

Research data are not shared.

Keywords

active carbon, adsorption, metal–organic frameworks, MOFs, porous materials, sulfur dioxide, zeolites

Received: December 10, 2020
Revised: January 12, 2021
Published online: February 11, 2021

[1] D. Gielen, R. Gorini, N. Wagner, R. Leme, L. Gutierrez, G. Prakash, E. Asmelash, L. Janeiro, G. Gallina, G. Vale, L. Sani, X. Casals, R. Ferroukhi, B. Parajuli, M. Renner, C. Garcia-Banos, J. Feng, *Global Energy Transformation: A Roadmap to 2050*, *IRENA*, Abu Dhabi **2019**.
[2] M. Maurya, J. K. Singh, *J. Phys. Chem. C* **2018**, *122*, 14654.
[3] F. Birol, L. Cozzi, T. Gould, S. Bouckaert, T.-Y. Kim, K. McNamara, B. Wanner, C. McGlade, P. Olejarnik, Z. Adam, L. Arboleya Sarazola, Y. Arsalane, B. Baruah, S. Bennett, M. Cappannelli, O. Chen, A. Contejean, H. Cisse Coulibaly, D. Crow, D. D'Ambrosio, A. Dasgupta, J. C. Donovan, M. Dos Santos, L. Gallarati, T. Goodson, L. Y. Lee, J. Liu, W. Matsumura, Y. Nobuoka, S. Papapanagiotou, C. Pavarini, D. Perugia, A. Petropoulos, A. Rouget, M. Ruiz de Chavez Velez, A. Schröder, G. Sondak, L. Staas, A. Toril, M. Waldron, M. A. Walton, W. Yu, P. Zeniewski, *International Energy Agency, World Energy Outlook 2019*, OECD Publishing, Paris **2019**.
[4] G. E. Likens, D. T. Driscoll, D. C. Buso, *Science* **1996**, *272*, 244.
[5] K. Gregory, C. Webster, S. Durk, *Energy Policy* **1996**, *24*, 655.
[6] R. K. Srivastava, W. Jozewicz, *J. Air Waste Manage. Assoc.* **2011**, *51*, 1676.
[7] J.-Y. Lee, T. C. Keener, Y. J. Yang, *J. Air Waste Manage. Assoc.* **2012**, *59*, 725.
[8] A. B. Rao, E. S. Rubin, *Environ. Sci. Technol.* **2002**, *36*, 4467.
[9] J. H. Goo, M. F. Irfan, S. D. Kim, S. C. Hong, *Chemosphere* **2007**, *67*, 718.
[10] S. Ding, F. Liu, X. Shi, K. Liu, Z. Lian, L. Xie, H. He, *ACS Appl. Mater. Interfaces* **2015**, *7*, 9497.
[11] P. K. Thallapally, R. K. Motkuri, C. A. Fernandez, B. P. McGrail, G. S. Behrooz, *Inorg. Chem.* **2010**, *49*, 4909.
[12] K. Tan, P. Canepa, Q. Gong, J. Liu, D. H. Johnson, A. Dyevoich, P. K. Thallapally, T. Thonhauser, J. Li, Y. J. Chabal, *Chem. Mater.* **2013**, *25*, 4653.
[13] T. Grant Glover, G. W. Peterson, B. J. Schindler, D. Britt, O. Yaghi, *Chem. Eng. Sci.* **2011**, *66*, 163.
[14] X. Han, S. Yang, M. Schröder, *Nat. Rev. Chem.* **2019**, *3*, 108.
[15] T. Jurado-Vázquez, E. Sánchez-González, A. E. Campos-Reales-Pineda, A. Islas-Jácome, E. Lima, E. González-Zamora, I. A. Ibarra, *Polyhedron* **2019**, *157*, 495.

[16] J. A. Zárate, E. Sánchez-González, D. R. Williams, E. González-Zamora, V. Martis, A. Martínez, J. Balmaseda, G. Maurin, I. A. Ibarra, *J. Mater. Chem. A* **2019**, *7*, 15580.
[17] R. Domínguez-González, I. Rojas-León, E. Martínez-Ahumada, D. Martínez-Otero, H. A. Lara-García, J. Balmaseda-Era, I. A. Ibarra, E. G. Percástegui, V. Jancik, *J. Mater. Chem. A* **2019**, *7*, 26812.
[18] Y. Zhang, Z. Chen, X. Liu, Z. Dong, P. Zhang, J. Wang, Q. Deng, Z. Zeng, S. Zhang, S. Deng, *Ind. Eng. Chem. Res.* **2019**, *59*, 874.
[19] S. Yang, J. Sun, A. J. Ramirez-Cuesta, S. K. Callear, W. I. F. David, D. P. Anderson, R. Newby, A. J. Blake, J. E. Parker, C. C. Tang, M. Schröder, *Nat. Chem.* **2012**, *4*, 887.
[20] X. Han, H. G. W. Godfrey, L. Briggs, A. J. Davies, Y. Cheng, L. L. Daemen, A. M. Sheveleva, F. Tuna, E. J. L. McInnes, J. Sun, C. Drathen, M. W. George, A. J. Ramirez-Cuesta, K. M. Thomas, S. Yang, M. Schröder, *Nat. Mater.* **2018**, *17*, 691.
[21] G. L. Smith, J. E. Eyley, X. Han, X. Zhang, J. Li, N. M. Jacques, H. G. W. Godfrey, S. P. Argent, L. J. McCormick McPherson, S. J. Teat, Y. Cheng, M. D. Frogley, G. Cinque, S. J. Day, C. C. Tang, T. L. Easun, S. Rudić, A. J. Ramirez-Cuesta, S. Yang, M. Schröder, *Nat. Mater.* **2019**, *18*, 1358.
[22] S. Yang, L. Liu, J. Sun, K. M. Thomas, A. J. Davies, M. W. George, A. J. Blake, A. H. Hill, A. N. Fitch, C. C. Tang, M. Schröder, *J. Am. Chem. Soc.* **2013**, *135*, 4954.
[23] M. Savage, Y. Cheng, T. L. Easun, J. E. Eyley, S. P. Argent, M. R. Warren, W. Lewis, C. Murray, C. C. Tang, M. D. Frogley, G. Cinque, J. Sun, S. Rudić, R. T. Murden, M. J. Benham, A. N. Fitch, A. J. Blake, A. J. Ramirez-Cuesta, S. Yang, M. Schröder, *Adv. Mater.* **2016**, *28*, 8705.
[24] V. Chernikova, O. Yassine, O. Shekhah, M. Eddaoudi, K. N. Salama, *J. Mater. Chem. A* **2018**, *6*, 5550.
[25] X. Cui, Q. Yang, L. Yang, R. Krishna, Z. Zhang, Z. Bao, H. Wu, Q. Ren, W. Zhou, B. Chen, H. Xing, *Adv. Mater.* **2017**, *29*, 1606929.
[26] P. Brandt, A. Nuhnen, M. Lange, J. Möllmer, O. Weingart, C. Janiak, *ACS Appl. Mater. Interfaces* **2019**, *11*, 17350.
[27] Z. Chen, X. Wang, R. Cao, K. B. Idrees, X. Liu, M. C. Wasson, O. K. Farha, *ACS Mater. Lett.* **2020**, *2*, 1129.
[28] C. Janiak, J. K. Vieth, *New J. Chem.* **2010**, *34*, 2366.
[29] M. P. Suh, H. J. Park, T. K. Prasad, D. W. Lim, *Chem. Rev.* **2012**, *112*, 782.
[30] K. Sumida, D. L. Rogow, J. A. Mason, T. M. McDonald, E. D. Bloch, Z. R. Herm, T.-H. Bae, J. R. Long, *Chem. Rev.* **2012**, *112*, 724.
[31] Y. He, W. Zhou, G. Qian, B. Chen, *Chem. Soc. Rev.* **2014**, *43*, 5657.
[32] D. Britt, D. Tranchemontagne, O. M. Yaghi, *Proc. Natl. Acad. Sci. U. S. A.* **2008**, *105*, 11623.
[33] N. S. Bobbitt, M. L. Mendonca, A. J. Howarth, T. Islamoglu, J. T. Hupp, O. K. Farha, R. Q. Snurr, *Chem. Soc. Rev.* **2017**, *46*, 3357.
[34] H. Wang, W. P. Lustig, J. Li, *Chem. Soc. Rev.* **2018**, *47*, 4729.
[35] E. Martínez-Ahumada, A. López-Olvera, V. Jancik, J. E. Sánchez-Bautista, E. González-Zamora, V. Martis, D. R. Williams, I. A. Ibarra, *Organometallics* **2020**, *39*, 883.
[36] T. Islamoglu, Z. Chen, M. C. Wasson, C. T. Buru, K. O. Kirlikovali, U. Afrin, M. R. Mian, O. K. Farha, *Chem. Rev.* **2020**, *120*, 8130.
[37] X. Shi, X. Zhang, F. Bi, Z. Zheng, L. Sheng, J. Xu, Z. Wang, Y. Yang, *J. Mol. Liq.* **2020**, *316*, 113812.
[38] X. Zhang, Y. Yang, L. Song, J. Chen, Y. Yang, Y. Wang, *J. Hazard. Mater.* **2019**, *365*, 597.
[39] a) J. J. Low, A. I. Benin, P. Jakubczak, J. F. Abrahamian, S. A. Faheem, R. R. Willis, *J. Am. Chem. Soc.* **2009**, *131*, 15834. b) K. Leus, T. Bogaerts, J. De Decker, H. Depauw, K. Hendrickx, H. Vrielinck, V. Van Speybroeck, P. Van Der Voort, *Microporous Mesoporous Mater.* **2016**, *226*, 110.
[40] M. R. Tchalala, P. M. Bhatt, K. N. Chappanda, S. R. Tavares, K. Adil, Y. Belmabkhout, A. Shkurenko, A. Cadiau, N. Heymans, G. Weireld, G. Maurin, K. N. Salama, M. Eddaoudi, *Nat. Commun.* **2019**, *10*, 1.
[41] Y. Zhang, P. Zhang, W. Yu, J. Zhang, J. Huang, J. Wang, M. Xu, Q. Deng, Z. Zeng, S. Deng, *ACS Appl. Mater. Interfaces* **2019**, *11*, 10680.
[42] D. Bahamon, A. Díaz-Márquez, P. Gamallo, L. F. Vega, *Chem. Eng. J.* **2018**, *342*, 458.
[43] W. Sun, L.-C. Lin, X. Peng, B. Smit, *AIChE J.* **2014**, *60*, 2314.
[44] X.-D. Song, S. Wang, C. Hao, J.-S. Qiu, *Inorg. Chem. Commun.* **2014**, *46*, 277.
[45] S. Bernt, V. Guillerm, C. Serre, N. Stock, *Chem. Commun.* **2011**, *47*, 2838.
[46] Y. Lin, C. Kong, L. Chen, *RSC Adv.* **2012**, *2*, 6417.
[47] G. Majano, O. Ingold, M. Yulikov, G. Jeschke, J. Pérez-Ramírez, *CrystEngComm* **2013**, *15*, 9885.
[48] A. Dhakshinamoorthy, M. Alvaro, P. Horcajada, E. Gibson, M. Vishnuvarthan, A. Vimont, J.-M. Grenèche, C. Serre, M. Daturi, H. Garcia, *ACS Catal.* **2012**, *2*, 2060.
[49] S. S.-Y. Chui, S. M.-F. Lo, J. P. H. Charmant, A. Guy Orpen, I. D. Williams, *Science* **1999**, *283*, 1148.
[50] M. Hartmann, S. Kunz, D. Himsl, O. Tangermann, S. Ernst, A. Wagener, *Langmuir* **2008**, *24*, 8634.
[51] a) X.-C. Huang, Y.-Y. Lin, J.-P. Zhang, X.-M. Chen, *Angew. Chem., Int. Ed.* **2006**, *45*, 1557. b) K. S. Park, Z. Ni, A. Côté, J. Y. Choi, R. Huang, F. J. Uribe-Romo, H. K. Chae, M. O'Keeffe, O. M. Yaghi, *Proc. Natl. Acad. Sci. U. S. A.* **2006**, *103*, 10186.
[52] Y. Hu, Z. Liu, J. Xu, Y. Huang, Y. Song, *J. Am. Chem. Soc.* **2013**, *135*, 9287.
[53] Q. Shi, Z. Chen, Z. Song, J. Li, J. Dong, *Angew. Chem., Int. Ed.* **2011**, *50*, 672.
[54] G. Zhong, D. Liu, J. Zhang, *J. Mater. Chem. A* **2018**, *6*, 1887.
[55] A. Srinivasan, M. W. Grutzeck, *Environ. Sci. Technol.* **1999**, *33*, 1464.
[56] B. M. Lok, C. A. Messina, R. L. Patton, R. T. Gajek, T. R. Cannan, E. M. Flanigen, *J. Am. Chem. Soc.* **1984**, *106*, 6092.
[57] P. Kuhn, M. Antonietti, A. Thomas, *Angew. Chem., Int. Ed.* **2008**, *47*, 3450.
[58] S. Kuroda, N. Tobori, M. Sakuraba, Y. Sato, *J. Power Sources* **2003**, *119–121*, 924.
[59] X. Qian, L. Jin, D. Zhao, X. Yang, S. Wang, X. Shen, D. Rao, S. Yao, Y. Zhou, X. Xi, *Electrochim. Acta* **2016**, *192*, 346.
[60] X. Hu, X. Lou, C. Li, Y. Ning, Y. Liao, Q. Chen, E. S. Mananga, M. Shen, B. Hu, *RSC Adv.* **2016**, *6*, 114483.
[61] S. D. Worrall, M. A. Bissett, P. I. Hill, A. P. Rooney, S. J. Haigh, M. P. Attfield, R. A. W. Dryfe, *Electrochim. Acta* **2016**, *222*, 361.
[62] C. A. C. Perez, N. S. de Resende, V. M. M. Salim, M. Schmal, *J. Phys. Chem. C* **2017**, *121*, 2755.
[63] H. Shi, *RSC Adv.* **2015**, *5*, 38330.
[64] D. Dutta, S. Chatterjee, K. T. Pillai, P. K. Pujari, B. N: Ganguly, *Chem. Phys.* **2005**, *312*, 319.
[65] S. Dey, S. Bügel, S. Sorribas, A. Nuhnen, A. Bhunia, J. Coronas, C. Janiak, *Front. Chem.* **2019**, *7*, 693.
[66] S. Öztürk, Y.-X. Xiao, D. Dietrich, B. Giesen, J. Barthel, J. Ying, Y.-X. Yang, C. Janiak, *Beilstein J. Nanotechnol.* **2020**, *11*, 770.
[67] Y. Zhao, K. X. Yao, B. Teng, T. Zhang, Y. Han, *Energy Environ. Sci.* **2013**, *6*, 3684.
[68] G. Wang, G. Sun, Q. Wang, S. Wang, J. Guo, Y. Gao, Q. Xin, *J. Power Sources* **2008**, *180*, 176.
[69] C. Mani-Lata, C. Hussakan, G. Panomsuwan, *J. Compos. Sci.* **2020**, *4*, 121.
[70] D. Jiang, L. L. Keenan, A. D. Burrows, K. J. Edler, *Chem. Commun.* **2012**, *48*, 12053.
[71] E. Martínez-Ahumada, M. L. Díaz-Ramírez, H. A. Lara-García, D. R. Williams, V. Martis, V. Jancik, E. Lima, I. A. Ibarra, *J. Mater. Chem. A* **2020**, *8*, 11515.
[72] M. Thommes, K. Kaneko, A. V. Neimark, J. P. Olivier, F. Rodriguez-Reinoso, J. Rouquerol, K. S. W. Sing, *Pure Appl. Chem.* **2015**, *87*, 1051.

[73] Ü. Kökçam-Demir, A. Goldman, L. Esrafili, M. Gharib, A. Morsali, O. Weingart, C. Janiak, *Chem. Soc. Rev.* **2020**, *49*, 2751.
[74] H. Bux, F. Liang, Y. Li, J. Cravillon, M. Wiebcke, J. Caro, *J. Am. Chem. Soc.* **2009**, *131*, 16000.
[75] W. Ma, Q. Jiang, P. Yu, L. Yang, L. Mao, *Anal. Chem.* **2013**, *85*, 7550.
[76] J.-R. Li, R. J. Kuppler, H.-C. Zhou, *Chem. Soc. Rev.* **2009**, *38*, 1477.
[77] M. E. Casco, Y. Q. Cheng, L. L. Deamen, D. Fairen-Jimenez, E. V. Ramos-Fernández, A. J. Ramirez-Cuesta, J. Silvestre-Albero, *Chem. Commun.* **2016**, *52*, 3639.
[78] R. M. Barrer, A. F. Denny, *J. Chem. Soc.* **1964**, 4684.
[79] S. G. Deng, Y. S. Lin, *Ind. Eng. Chem. Res.* **1995**, *34*, 4063.
[80] A. Sultana, D. D. Habermacher, C. E. A. Kirschhock, J. A. Martens, *Appl. Catal., B* **2004**, *48*, 65.
[81] L. Manying, G. Liping, J. Shangbin, T. Bien, *J. Mater. Chem. A* **2019**, *7*, 5153.
[82] S. Glomb, D. Woschko, G. Makhloufi, C. Janiak, *ACS Appl. Mater. Interfaces* **2017**, *9*, 37419.
[83] J. H. Carter, X. Han, F. Y. Moreau, I. da Silva, A. Nevin, H. G. W. Godfrey, C. C. Tang, S. Yang, M. Schröder, *J. Am. Chem. Soc.* **2018**, *140*, 15564.
[84] N. F. Cessford, N. A. Seaton, T. Düren, *Ind. Eng. Chem. Res.* **2012**, *51*, 4911.
[85] 3P INSTRUMENTS, 3P sim, Version 1.1.0.7, Simulation and Evaluation Tool for mixSorb, 3P INSTRUMENTS **2018**.
[86] G. W. Peterson, J. A. Rossin, J. B. DeCoste, K. L. Killops, M. Browe, E. Valdes, P. Jones, *Ind. Eng. Chem. Res.* **2013**, *52*, 5462.
[87] W. P. Mounfield, C. Han, S. H. Pang, U. Tumuluri, Y. Jiao, S. Bhattacharyya, M. R. Dutzer, S. Nair, Z. Wu, R. P. Lively, D. S. Sholl, K. S. Walton, *J. Phys. Chem. C* **2016**, *120*, 27230.
[88] C. Prestipino, L. Regli, J. G. Vitillo, F. Bonino, A. Damin, C. Lamberti, A. Zecchina, P. L. Solari, K. O. Kongshaug, S. Bordiga, *Chem. Mater.* **2006**, *18*, 1337.
[89] J. Szanyi, M. Daturi, G. Clet, D. R. Baer, C. H. Peden, *Phys. Chem. Chem. Phys.* **2012**, *14*, 4383.
[90] C. Chen, T. Wu, H. Wu, H. Liu, Q. Qian, Z. Liu, G. Yang, B. Han, *Chem. Sci.* **2018**, *9*, 8890.
[91] S. Bordiga, L. Regli, F. Bonino, E. Groppo, C. Lamberti, B. Xiao, P. S. Wheatley, R. E. Morris, A. Zecchina, *Phys. Chem. Chem. Phys.* **2007**, *9*, 2676.
[92] C. Beauvais, A. Boutin, A. H. Fuchs, *C. R. Chim.* **2005**, *8*, 485.
[93] A. Malka-Edery, K. Abdallah, P. Grenier, F. Meunier, *Adsorption* **2001**, *7*, 17.
[94] C. Mellot-Draznieks, J. Rodriguez-Carvajal, D. E. Cox, A. K. Cheetham, *Phys. Chem. Chem. Phys.* **2003**, *5*, 1882.